

Carbon Recombination Lines near 327 MHz

I: “Diffuse” C II regions in the Galactic Disk

D. Anish Roshi^{1,2} *, N. G. Kantharia², and K. R. Anantharamaiah^{3**}

¹ National Radio Astronomy Observatory, Green Bank, WV 24944, USA.

² National Centre for Radio Astrophysics, Tata Institute of Fundamental Research, Pune, India

³ Raman Research Institute, Bangalore, India

Received / Accepted

Abstract. In earlier papers (Roshi & Anantharamaiah 2000, 2001a), we presented extensive surveys (angular resolution – $2^\circ \times 2^\circ$ & $2^\circ \times 6'$) of radio recombination lines (RRLs) near 327 MHz in the longitude range $l = 332^\circ \rightarrow 89^\circ$ using the Ooty Radio Telescope. These surveys have detected carbon lines mostly between $l = 358^\circ \rightarrow 20^\circ$ and in a few positions at other longitudes. This paper presents the observed carbon line parameters in the high-resolution survey and a study of the galactic distribution and angular extent of the line emission observed in the surveys. The carbon lines detected in the surveys arise in “diffuse” C II regions. The l - v diagram and radial distribution constructed from our carbon line data shows similarity with that obtained from hydrogen recombination lines at 3 cm from H II regions indicating that the distribution of the diffuse C II regions in the inner Galaxy resembles the distribution of the star-forming regions. We estimated the [C II] $158\mu\text{m}$ emission from diffuse C II regions and find that upto 95 % of the total observed [C II] $158\mu\text{m}$ emission can arise in diffuse C II regions if the temperature of the latter ~ 80 K. Our high-resolution survey data shows that the carbon line emitting regions have structures on angular scale $\sim 6'$. Analysis of the dual-resolution observations toward a 2° wide field centered at $l = 13^\circ.9$ and toward the longitude range $l = 1^\circ.75$ to $6^\circ.75$ shows the presence of narrow ($\Delta V \leq 15$ km s⁻¹) carbon line emitting regions extending over several degrees in l and b . The physical size perpendicular to the line-of-sight of an individual diffuse C II region in these directions is > 200 pc.

Key words. Galaxy: general – C II regions – ISM: general – ISM: structure – radio lines: ISM – infrared: ISM

1. Introduction

Radio recombination lines (RRLs) of hydrogen, helium and carbon have been unambiguously identified in the spectra obtained toward H II regions (see review by Roelfsema & Goss 1992). The hydrogen and helium recombination lines mostly originate in hot ($T_e \sim 5000 - 10000$ K) regions ionized by photons of energy ≥ 13.6 eV. Since the ionization potential of carbon is 11.4 eV, low energy photons ($11.4 \text{ eV} \leq E < 13.6 \text{ eV}$) that escape from H II regions can ionize gas phase carbon atoms outside the hot regions. Thus ionized carbon regions can exist in dense (hydrogen nucleus density $n_0 \sim 10^5 \text{ cm}^{-3}$) photo-dissociation regions (PDRs) adjacent to H II regions or in the neutral components (H I or molecular) of the in-

terstellar medium (ISM). Tielens and Hollenbach (1985) define PDRs as regions where the heating or/and chemistry of the predominantly neutral gas is governed by the FUV (6–13.6 eV) photons. Since the FUV photons are omnipresent, the PDRs, by definition encompass a substantial fraction of atomic gas in a galaxy (Hollenbach & Tielens 1997 and references therein). The dense PDRs (Tielens & Hollenbach 1985) are located at the interface of molecular clouds and H II regions whereas the low-density ($n_0 \sim 10^3 \text{ cm}^{-3}$) PDRs (Hollenbach, Takahashi & Tielens 1991) are located in the diffuse interstellar gas; the ambient FUV flux sufficing to control its chemistry and heating. The ionized carbon regions in the dense PDRs are referred to as “classical” C II regions. These C II regions are observationally identified by the narrow ($1 - 10 \text{ km s}^{-1}$) emission lines of carbon at frequencies > 1 GHz. Several studies have been made to understand and model the line emission from such regions (eg. Garay et al. 1998, Wyrowski et al. 2000). These regions are not accessible to low frequency RRLs due to the increased pressure broadening ($\propto \nu^{-8.2/3}$; Shaver 1975) and increased

Send offprint requests to: D. Anish Roshi e-mail: aroshi@nrao.edu

* On leave from National Centre for Radio Astrophysics, Tata Institute of Fundamental Research, Pune, India

** We regret to announce that our friend and collaborator, K. R. Anantharamaiah passed away on 29 October, 2001 before this work could be completed

free-free continuum optical depths ($\tau \propto \nu^{-2}$). The second class of C II regions, referred to as “diffuse” C II regions, coexists with the diffuse neutral component of the ISM. The emission measures of these regions are fairly low ($< 0.1 \text{ cm}^{-6}\text{pc}$; Kantharia, Anantharamaiah & Payne 1998) and hence these regions are observable in low-frequency RRLs of carbon as either absorption lines or emission lines due to stimulated emission from inverted populations. The diffuse C II regions, observed in carbon lines at frequencies $< 1 \text{ GHz}$, are the focus of this paper.

The diffuse C II region located in the Perseus arm toward the strong radio continuum source, Cas A has been extensively studied using low frequency recombination lines of carbon. In fact, most of our knowledge on this class of C II regions has come from these observations. Konovalenko & Sodin (1980) were the first to observe a low-frequency (26.3 MHz) absorption line toward Cas A, which was later correctly identified as the 631α recombination line of carbon by Blake, Crutcher & Watson (1980). Since then, several recombination line observations spanning over 14 to 1400 MHz have been made toward this direction (Kantharia et al. 1998 and references therein). The predicted smooth transition of carbon lines in absorption at frequencies below 115 MHz to lines in emission at frequencies above 200 MHz has been demonstrated toward this direction (Payne, Anantharamaiah & Erickson 1989). The extensive RRL data collected toward Cas A has been used in modeling the line-forming gas. The models show that the carbon RRLs originate in small, relatively cool tenuous regions ($T_e = 35\text{--}75 \text{ K}$, $n_e = 0.05\text{--}0.1 \text{ cm}^{-3}$, size $\sim 2 \text{ pc}$; Payne, Anantharamaiah & Erickson 1994) of the ISM. Comparison of the distribution of carbon RRLs near 327 MHz observed with the VLA ($2'.7 \times 2'.4$) toward Cas A with H I absorption in the same direction suggests that the carbon line-forming region likely coexists with the cold, diffuse H I component of the ISM (Anantharamaiah et al. 1994).

In addition to the region toward Cas A, the distribution of the diffuse C II regions in the Galaxy has also been studied to some extent. Surveys have been conducted near 76 MHz ($n \sim 441$) with the Parkes 64m telescope (Erickson, McConnell & Anantharamaiah 1995) and near 35 MHz ($n \sim 580$) with the Gauribidanur telescope (Kantharia & Anantharamaiah 2001) to search for carbon recombination lines, mostly in the inner part of the Galaxy. These observations have succeeded in detecting carbon RRLs in absorption from several directions in the galactic plane with longitudes ranging from $l = 340^\circ \rightarrow 20^\circ$. The diffuse C II regions appear to be fairly widespread in the inner part of our Galaxy. Observations away from the Galactic plane have shown the region to be several degrees wide in galactic latitude. The positions with detections near 35 MHz were observed near 327 MHz using the Ooty Radio Telescope by Kantharia & Anantharamaiah (2001) and the emission counterparts of the carbon absorption lines were detected. Combining their observations with all other existing carbon RRL observations, they modeled the line emission at different po-

sitions in the galactic plane. While models with physical properties similar to those obtained in the direction of Cas A can fit the observed data, the possibility of carbon lines originating in regions with temperature $\leq 20 \text{ K}$ cannot be ruled out (Kantharia & Anantharamaiah 2001). If the temperature of the diffuse C II regions is found to be low, then these regions could even be associated with the molecular component of the ISM (Konovalenko 1984, Golynkin & Konovalenko 1990, Sorochev 1996, Kantharia & Anantharamaiah 2001). These low temperature regions may be low-density PDRs (Hollenbach, Takahashi, Tielens 1991) formed on surfaces of molecular clouds due to ionization from background FUV radiation. Although some modeling of these diffuse C II regions using low-frequency carbon RRLs has been done, a wide range of parameter space has been found to fit the existing observations. The physical properties, distribution and association of these regions with other components of the ISM requires more investigation. In addition to carbon RRLs, ionized carbon is also traced by the [C II] $158\mu\text{m}$ line. The $158\mu\text{m}$ line emission from the Galaxy has been mapped by Bennett et al. (1994) and Nakagawa et al. (1998). They find that the [C II] $158\mu\text{m}$ emission consists of compact emission regions associated with compact H II regions (Nakagawa et al. 1998) and a diffuse emission whose origin is not very clear. Since both the fine-structure line and the carbon RRLs require ionized carbon regions, it is possible that the two can arise from similar regions. Kantharia & Anantharamaiah (2001) tried to compare the carbon lines near 35 MHz with the [C II] $158\mu\text{m}$ emission but they did not derive any conclusive results. Hence, no detailed comparative study of the radio and FIR line emission of carbon from diffuse C II regions exists. In this paper, we also attempt a discussion on these two tracers of ionized carbon regions.

Extensive surveys of recombination lines near 327 MHz have been made with the primary objective to study the low-density ionized gas in the Galaxy by observing low-frequency hydrogen RRLs from this gas (Roshi & Anantharamaiah 2000; hereafter Paper I; Roshi & Anantharamaiah 2001a; hereafter Paper II; Roshi & Anantharamaiah 2001b). Since the velocity coverage of these surveys was sufficient to allow detection of carbon RRLs, which are separated from the hydrogen line by $\sim -150 \text{ km s}^{-1}$, the surveys have succeeded in detecting carbon features toward several positions in the galactic plane. The surveys have data with two different angular resolutions obtained by using the Ooty Radio Telescope in two different operating modes (see Paper I & II). The carbon line data obtained from the higher angular resolution observation ($2^\circ \times 6'$) are presented in this paper (see Paper II for spectra) and those obtained in the lower resolution ($2^\circ \times 2^\circ$) survey were presented in Paper I. In this paper, we present a study of the distribution and angular extent of the carbon line forming region in the galactic plane by making use of the carbon RRLs detected in the 327 MHz surveys. Interestingly, in several directions the carbon line emission observed in the surveys seems to be

associated with H I self-absorption features, which will be discussed in Roshi, Kantharia & Anantharamaiah (2002).

A summary of the observations and basic results are presented in Section 2. Section 3 discusses the distribution of the diffuse C II regions in the galactic disk and compares it with the distribution of other components of the ISM. Section 4 discusses the possibility of a common origin of the carbon RRL and the diffuse [C II] $158\mu\text{m}$ line emission. The latitude extent of carbon line emission is discussed in Section 5. The higher resolution observations are used to study the angular extent of the carbon line emitting region, which is discussed in Section 6. Section 7 summarizes the paper.

2. Summary of Observations and Basic Results

The RRL surveys, which were described in detail in Papers I & II, were made using the Ooty Radio Telescope (ORT). ORT is a $530\text{m} \times 30\text{m}$ parabolic cylinder operating at a nominal center frequency of 327 MHz (Swarup et al. 1971). The observations were made with two different angular resolutions – (a) $2^\circ \times 2^\circ$ (low resolution mode) and (b) $2^\circ \times 6'$ (high resolution mode). The high resolution mode is obtained by using all the 22 ‘modules’ of the ORT, which together form a telescope of size $530\text{m} \times 30\text{m}$, and the low resolution mode is obtained by using only a single ‘module’ of the ORT, which effectively is a telescope of size $24\text{m} \times 30\text{m}$. The RRL transitions from principal quantum numbers $n = 270, 271, 272$ and 273 and $\Delta n = 1$ were simultaneously observed using a multi-line spectrometer (Roshi 1999). The final spectrum is obtained by averaging all the four RRL transitions.

2.1. Low-resolution Survey

In the low-resolution survey (Paper I), 51 positions were observed in the inner Galaxy: longitude range $l = 332^\circ$ to 0° to 89° and $b = 0^\circ$. The positions were separated in longitude by $\sim 2^\circ \times \sec(\delta)$, δ being the declination. Carbon RRLs were detected from almost all directions in the longitude range $l = 358^\circ \rightarrow 20^\circ$ and also from a few positions in the longitude range $l = 20^\circ$ to 89° . In the outer Galaxy ($172^\circ < l < 252^\circ$) a total of 14 positions, spaced by $\sim 5^\circ - 7^\circ$ in longitude, were observed. However, no carbon RRLs were detected in this longitude range. At two specific longitudes in the inner Galaxy ($l = 0^\circ.0$ & $13^\circ.9$), spectra were taken in steps of 1° up to $b = \pm 4^\circ$ to study the latitude extent of the carbon line emission. The observed spectra and line fit parameters were presented in Paper I.

2.2. High-resolution Survey

In the high-resolution survey (Paper II), a set of seven fields which were 2° wide and two fields which were $6'$ wide in longitude were observed with a $2^\circ \times 6'$ beam. The fields are designated as Field 1 to 9 and are centered at $l = 348^\circ.0$ (2° wide), $3^\circ.4$ ($6'$), $13^\circ.9$ (2°), $25^\circ.2$ (2°),

$27^\circ.5$ (2°), $36^\circ.3$ ($6'$), $45^\circ.5$ (2°), $56^\circ.9$ (2°) and $66^\circ.2$ (2°) respectively. The ORT is an equatorially mounted telescope and the beam size is 2° along right ascension. The orientation of the beam with respect to galactic coordinates, therefore, changes as a function of galactic longitude. Carbon RRLs were detected toward several positions within the fields with $l < 40^\circ$, whereas no lines were detected at any individual positions within the fields in the longitude range $l = 40^\circ$ to 85° . The galactic coordinates of the positions where carbon lines are detected and the parameters estimated from Gaussian fits to the line profiles are given in Table 1. Each spectrum was inspected by eye and the presence of a carbon line was determined. If narrow ($\sim 1\text{-}2$ channels) spectral features were present in addition to the carbon line feature, we regarded the detection as tentative. The narrow spurious features were either due to residual radio frequency interference or “bad” spectral channel values, which were inferred from the channel weights as discussed in Paper I. However, if the width of the carbon line was several times (~ 10) larger than any spurious narrow features then we regarded them as real. Since the peak line intensity to the RMS noise in the spectra is about 3 to 4, care has been taken in fitting Gaussian components to the line profile. A second Gaussian component was fitted to only those spectra where the residuals left after removing a single Gaussian component were inconsistent with the noise in rest of the spectrum. The details of the high-resolution survey and the observed spectra were presented in Paper II.

2.3. Line Width

If we assume that the physical properties of the carbon line emitting gas observed in the galactic disk are similar to those derived for the gas toward Cas A (e.g. $T_e = 75\text{K}$, $n_e = 0.1\text{ cm}^{-3}$, from Payne et al. 1994) and the galactic background radiation temperature = 700 K (from Paper I), then the total contribution from pressure, radiation and Doppler broadening at 325 MHz would be a negligible $\sim 0.6\text{ km s}^{-1}$. Comparing this with the observed line widths in the high-resolution data ranging from 4 to 48 km s^{-1} with a median value of 14 km s^{-1} (Fig. 1), it is clear that the cause of line broadening lies elsewhere. Blending of carbon line features from different line forming regions within the coarse survey beam and turbulent motions within the cloud are likely the cause of the broad lines. To confirm this we have examined the data toward a few directions in the galactic plane in more detail and the results (see Section 6 for details) support our conclusion. Moreover, the median line width obtained from the low-resolution survey data is 17 km s^{-1} (Paper I), which is somewhat larger than the value estimated from the higher resolution data ($\sim 14\text{ km s}^{-1}$). The larger median value is likely a result of line blending because of the relatively larger beam width of the low-resolution survey. The line widths of carbon lines observed in the survey are typically a factor of 2 to 5 larger than the typical line width of car-

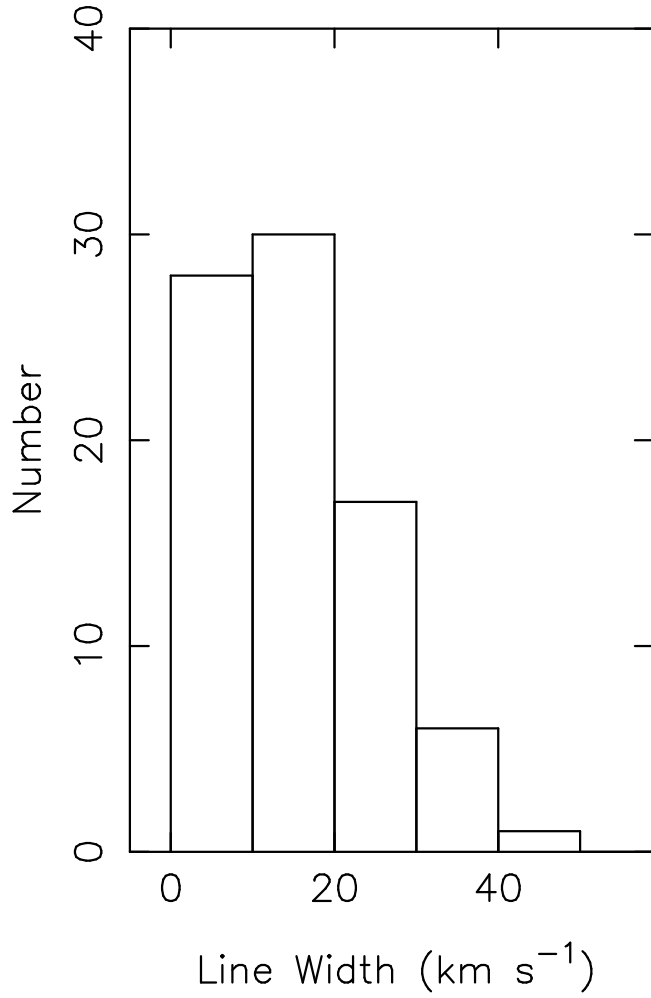


Fig. 1. Histogram of the observed carbon line widths in the high-resolution ($2^\circ \times 6'$) survey data.

bon lines observed at frequencies > 1 GHz from “classical” C II regions (eg. Roelfsema & Goss 1992). Since the lines at low and high frequencies are believed to arise in distinct regions of the ISM, the difference is not surprising.

Table 1. Summary of the carbon RRL observations from the high resolution survey

l °	b °	T_L/T_{sys}^1 $\times 10^3$	ΔV km s $^{-1}$	V_{LSR} km s $^{-1}$	V_{res}^2 km s $^{-1}$	RMS 3 $\times 10^3$	t_{int} hrs
Field 2a							
0.52	+0.03	0.64(0.08)	22.4(3.2)	1.7(1.4)	1.8	0.20	12.8
0.67	−0.00	0.66(0.18)	4.3(1.3)	6.7(0.6)	1.8	0.19	11.2
		0.37(0.15)	5.8(2.7)	−11.1(1.2)	1.8	0.19	11.2
0.75	+0.05	0.54(0.11)	9.8(2.3)	18.9(1.0)	3.4	0.13	11.6
		0.41(0.09)	14.8(3.7)	−7.2(1.6)	3.4	0.13	11.6
0.84	+0.10	0.69(0.12)	15.0(3.0)	6.3(1.3)	3.4	0.18	9.4
0.92	+0.16	0.83(0.22)	4.0(1.2)	6.5(0.5)	1.8	0.23	12.6
Field 2b (G2.3+0.0)							
1.21	+0.07	0.32(0.1) ⁴	11.1(4.2)	2.6(1.7)	3.4	0.13	10.3
		0.33(0.11) ⁴	9.2(3.6)	−17.8(1.5)	3.4	0.13	10.3
1.29	+0.13	0.58(0.08)	25.5(4.2)	3.6(1.8)	2.1	0.21	9.9
1.38	+0.18	0.55(0.08)	30.1(5.3)	1.6(2.2)	3.4	0.17	10.1
1.83	+0.20	0.63(0.15)	7.3(2.0)	1.9(0.9)	2.1	0.20	11.3
2.29	+0.21	0.47(0.09)	14.3(3.1)	10.3(1.3)	2.1	0.17	14.9
2.54	−0.03	0.53(0.13)	14.3(4.0)	8.9(1.7)	2.1	0.24	8.1
2.63	+0.02	0.55(0.12)	10.3(2.6)	4.0(1.1)	2.1	0.19	11.2
2.78	−0.03	0.34(0.08)	18.0(4.6)	11.1(1.9)	2.1	0.16	11.2
2.86	+0.02	0.32(0.07)	28.7(7.9)	10.6(3.3)	2.1	0.20	12.5
3.01	−0.03	0.44(0.08)	26.3(5.3)	9.3(2.2)	2.1	0.19	11.2
3.09	+0.02	0.49(0.12)	12.8(3.6)	5.8(1.5)	2.1	0.21	11.7
3.33	+0.02	0.46(0.1)	14.0(3.7)	6.9(1.5)	2.1	0.19	11.5
Field 2c (G4.7+0.0)							
3.56	+0.02	0.33(0.08)	19.5(5.3)	10.0(2.2)	3.4	0.13	10.4
3.79	+0.02	0.45(0.12)	11.8(3.6)	9.8(1.5)	3.4	0.16	11.6
3.94	−0.03	0.66(0.15)	8.8(2.3)	11.6(1.0)	2.1	0.22	8.4
4.26	+0.02	0.72(0.15)	7.8(1.9)	5.8(0.8)	2.1	0.21	12.2
4.49	+0.02	0.40(0.12) ⁴	14.4(5.0)	9.2(2.1)	3.4	0.17	11.6
4.64	−0.03	0.27(0.08) ⁴	22.8(7.9)	8.0(3.3)	3.4	0.15	9.6
4.72	+0.02	0.39(0.09)	28.2(7.5)	10.6(3.2)	3.4	0.18	11.5
4.87	−0.03	0.79(0.18) ⁴	7.0(1.9)	11.9(0.8)	1.8	0.25	8.3
		0.75(0.22) ⁴	4.9(1.6)	−35.5(0.7)	1.8	0.25	8.3
4.95	+0.02	0.64(0.14)	11.4(2.8)	9.0(1.2)	2.1	0.23	8.5
5.19	+0.02	0.78(0.15)	8.1(1.8)	8.4(0.8)	1.8	0.23	9.0
5.33	−0.03	0.54(0.07)	22.6(3.6)	12.8(1.5)	2.1	0.17	10.2
5.42	+0.02	0.49(0.09)	20.1(4.0)	9.1(1.7)	2.1	0.19	10.6
5.56	−0.03	0.71(0.19) ⁴	4.3(1.4)	7.5(0.6)	2.1	0.20	10.0
5.65	+0.02	0.79(0.15)	7.1(1.5)	5.6(0.6)	2.1	0.19	12.3
5.80	−0.03	0.80(0.15)	9.1(1.9)	5.2(0.8)	2.1	0.22	7.4
		0.72(0.19)	5.5(1.7)	18.4(0.8)	2.1	0.22	7.4
5.88	+0.02	0.51(0.13)	14.0(4.0)	13.7(1.7)	2.1	0.23	8.6
6.02	−0.02	0.43(0.14) ⁴	20.3(7.7)	6.0(3.2)	3.4	0.24	4.2
6.25	−0.02	0.67(0.14) ⁴	16.0(3.9)	0.6(1.6)	2.1	0.27	5.6
6.72	−0.02	0.53(0.12)	9.7(2.6)	6.1(1.1)	2.1	0.19	10.0
6.80	+0.03	0.58(0.12)	8.6(2.0)	7.7(0.9)	2.1	0.17	11.4

Field 3 (G13.9+0.0)							
13.04	−0.46	0.46(0.07)	36.0(6.6)	40.6(2.8)	2.1	0.21	7.9
13.13	−0.41	0.46(0.14)	7.0(2.5)	52.1(1.0)	2.1	0.18	10.6
		0.89(0.11)	10.8(1.6)	35.2(0.7)	2.1	0.18	10.6
		0.64(0.11)	12.5(2.4)	15.7(1.0)	2.1	0.18	10.6
13.22	−0.36	0.41(0.08)	37.2(8.1)	39.9(3.4)	1.8	0.24	8.2
		0.61(0.16)	8.0(2.5)	18.4(1.1)	1.8	0.24	8.2
13.30	−0.31	0.51(0.1)	24.8(5.8)	42.3(2.4)	1.8	0.26	8.4
		0.99(0.17)	8.6(1.7)	19.8(0.7)	1.8	0.26	8.4
13.39	−0.26	0.44(0.12)	14.4(4.6)	11.8(2.0)	2.1	0.23	8.4
		0.33(0.09)	29.8(8.8)	39.5(3.7)	2.1	0.23	8.4
13.48	−0.22	0.38(0.11)	28.6(9.7)	44.0(4.1)	3.4	0.23	11.2
		0.50(0.15)	16.5(5.6)	14.5(2.4)	3.4	0.23	11.2
13.57	−0.17	0.77(0.18)	5.4(1.5)	19.3(0.6)	2.1	0.21	9.3
		0.43(0.07)	38.9(7.0)	33.1(3.0)	2.1	0.21	9.3
13.65	−0.12	0.41(0.09)	20.8(5.4)	24.8(2.3)	2.1	0.20	9.1
13.74	−0.07	0.57(0.17) ⁴	9.0(3.2)	18.0(1.3)	2.1	0.25	8.0
13.83	−0.02	0.49(0.14) ⁴	10.1(3.3)	44.5(1.4)	2.1	0.21	8.8
		0.66(0.19) ⁴	5.2(1.8)	18.7(0.7)	2.1	0.21	8.8
13.92	+0.03	0.84(0.21) ⁴	6.5(1.9)	19.2(0.8)	2.1	0.26	6.3
14.09	+0.12	0.45(0.05)	47.3(6.3)	34.3(2.7)	2.1	0.18	10.0
14.18	+0.17	0.35(0.09)	19.1(5.7)	39.8(2.4)	2.1	0.19	10.9
		0.61(0.13)	8.6(2.2)	19.6(0.9)	2.1	0.19	10.9
14.36	+0.26	0.58(0.06)	29.3(3.6)	43.6(1.5)	2.1	0.16	11.7
		0.57(0.1)	11.3(2.3)	18.7(1.0)	2.1	0.16	11.7
14.44	+0.31	0.52(0.08)	27.1(5.1)	19.6(2.1)	2.1	0.21	7.5
14.62	+0.41	0.52(0.14)	9.9(3.1)	26.9(1.3)	2.1	0.22	10.1
14.71	+0.46	0.35(0.1)	12.8(4.4)	51.5(1.9)	2.1	0.18	11.8
		0.43(0.08)	20.0(4.5)	23.0(1.9)	2.1	0.18	11.8
Field 5 (G27.5+0.0)							
27.06	−0.20	0.41(0.09)	19.4(5.1)	58.2(2.2)	3.4	0.16	8.0
28.04	+0.31	0.66(0.15)	6.6(1.7)	79.5(0.7)	1.8	0.20	15.0
28.13	+0.35	0.34(0.07)	20.7(5.1)	73.2(2.2)	3.4	0.13	18.6
Field 6a (G34.2+0.0)							
34.18	−0.02	0.63(0.15) ⁴	8.1(2.3)	44.4(1.0)	2.1	0.22	9.7
34.27	+0.03	0.36(0.08)	15.2(3.9)	49.2(1.6)	2.1	0.15	13.1
34.85	−0.02	0.55(0.08)	31.3(5.6)	43.8(2.3)	2.1	0.23	8.9
34.94	+0.03	0.45(0.1)	18.1(4.7)	41.0(2.0)	2.1	0.21	11.0
35.08	−0.02	0.38(0.1)	17.4(5.0)	51.6(2.1)	3.4	0.15	8.9
35.17	+0.03	0.51(0.08)	26.6(5.1)	50.2(2.2)	3.4	0.17	11.9
35.31	−0.02	0.23(0.07)	19.1(7.0)	66.4(2.9)	7.6	0.82	11.1
Field 6b (G36.5+0.0)							
35.76	−0.02	0.56(0.10)	12.6(2.5)	51.5(1.0)	2.1	0.17	10.7
36.21	−0.02	0.43(0.07)	30.3(5.5)	52.7(2.3)	2.1	0.18	10.5

¹ The line intensities are given in units of T_L/T_{sys} , where T_L is the line antenna temperature and T_{sys} is the system temperature, which includes sky, receiver and spillover temperature

² The spectral resolution in km s^{-1} .

³ RMS is in units of T_L/T_{sys} .

⁴ Tentative detection.

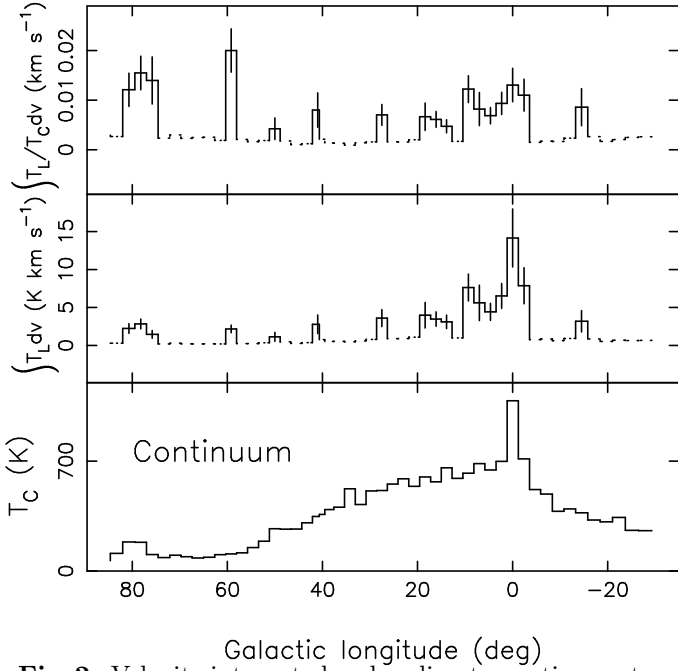


Fig. 2. Velocity integrated carbon line-to-continuum temperature ratio (top panel), velocity-integrated carbon line temperature (middle panel) and the continuum emission (bottom panel) near 327 MHz, observed in the low-resolution ($2^\circ \times 2^\circ$) survey, plotted as a function of galactic longitude. The horizontal lines in the top and middle panels indicate the observed positions where carbon lines are detected. The vertical bar represents the 3σ uncertainty in the plotted parameters. The dashed line in these plots indicate observed positions with no detections and give the upper limit on the quantities plotted. These limits were estimated from the RMS noise (σ) on the spectra and assuming a typical width for the carbon line as 17 km s^{-1} . The continuum temperature plotted in the bottom panel is the measured antenna temperature corrected for the beam efficiency factor (0.65) and is same as T_C discussed in Section 3.1 under the assumptions stated in that section.

3. Distribution of the Carbon Line Forming Gas in the Galactic disk

3.1. Observed Longitudinal Variation of Integrated Line Intensity

The variation of velocity-integrated line-to-continuum temperature ratio, velocity-integrated line strength of carbon RRLs and continuum temperature with galactic longitude observed in the low-resolution survey is shown in Fig. 2. The line-to-continuum ratio for optically thin case is approximately given by (Shaver 1975),

$$\frac{T_L}{T_C} \sim -\tau_L + \frac{T_e \tau_L}{T_C \beta_n}, \quad (1)$$

where T_L , T_C and T_e are the line brightness temperature, continuum brightness temperature and electron tempera-

ture respectively and τ_L is the non-LTE line optical depth. $\beta_n \sim 1 - \frac{kT_e}{h\nu} \frac{d \ln(b_n)}{dn}$ for $\Delta n = 1$ transition. Here k is the Boltzmann's constant, h is the Planck's constant, ν is the frequency of the line emission and b_n is the departure coefficient. β_n is a measure of the non-LTE effects on the level populations. For getting Eq. 1, it is also assumed that the beam dilution is negligible and the measured continuum temperature is approximately the background temperature at the location of the line-forming region. Since $-\beta_n \sim 50 - 100$ at levels near $n \sim 272$ for typical physical conditions of the line-forming region, the line-to-continuum ratio is approximately the line optical depth even for the case where $T_e \sim T_C$. If we assume that beam dilution is negligible and the background temperature is the measured continuum temperature, both of which might not be true for all longitudes, then we can conclude that the top panel of Fig. 2 shows the variation of velocity-integrated line optical depth with longitude. If the assumptions are not valid, then the plotted values will be the apparent integrated optical depth which would be a lower limit on the actual integrated optical depth. The integrated optical depth (top panel in Fig. 2) is constant ($\sim 0.01 \text{ km s}^{-1}$) within 3σ measurement errors for most of our detections. From the top and middle panels, it is evident that line emission is concentrated in the longitude range $358^\circ \rightarrow 20^\circ$ with a few detections at longitudes between 20° and 89° . The strongest integrated line strength and continuum are observed toward the Galactic center. This is a good case of stimulated emission; the optical depth toward this region is not enhanced as compared to the neighboring longitudes. The bump near $l = 80^\circ$ (see Fig. 2) seen in all three distributions is from the gas associated with the well-known Cygnus complex located in the nearby Orion spiral arm. There are only a couple of detections in the fourth quadrant.

After examining the observed distribution of the line emission with longitude (Fig. 2) and various factors at play, we conclude that the paucity of detections at longitudes outside the range $358^\circ < l < 20^\circ$ may not be real but a result of one or more of the following selection effects: 1) reduced background radiation field leading to reduced stimulated emission and hence weaker lines. This, we believe is the reason for fewer detections at longitudes $> 20^\circ$. Since the intensity of carbon RRLs is amplified by the non-thermal background continuum due to stimulated emission (Paper I), the gradual drop in the non-thermal continuum with increasing longitudes might be partially responsible for the drop in the line strengths and subsequently lesser number of detections between longitudes 20° and 80° . 2) Beam dilution within the large low resolution survey beam leading to reduced line strengths and our sensitivity-limited sample failing to detect these lines. This is likely the dominant cause of non-detection of lines in the fourth quadrant. The ORT has an equatorial mount and electrical phasing is used to point the telescope along the declination axis. At longitudes $l < 355^\circ$ due to a variety of reasons (eg. improper phasing) the telescope

sensitivity drops and also the beam size increases (Roshi 1999). The drop in the continuum temperature at these longitudes (Fig. 2) is a result of this effect. On the other hand, negligible beam dilution effects could be one of the reasons we detect the carbon lines from the Cygnus region ($l \sim 80^\circ$) located in the nearby Orion arm despite the background radiation field being weaker than the regions between $l = 20^\circ$ to 80° and the presence of increased beam size as in negative longitudes.

The few positions where carbon lines were detected in the longitude range 20° to 80° show the presence of either H II regions or supernova remnants within the $2^\circ \times 2^\circ$ region centered at these positions, which suggests that the carbon line emission might be associated with star forming regions. Moreover, these detections appear at velocities close to the tangent point velocities at those longitudes. The long path lengths near the tangent points might have favored the detection of carbon lines in these directions. Higher sensitivity observations of these regions should show more detections in this longitude range if this is the case. Indeed, our high-resolution survey data has detected carbon lines at several positions between $l = 20^\circ$ to 38° as listed in Table 1. This clearly indicates that diffuse C II regions exist in this longitude range and the selection effects noted above are likely responsible for their non-detections in the low-resolution survey.

3.2. l - v diagram

The longitude-velocity diagram constructed from RRL observations of the galactic plane can be used to understand the distribution of the carbon line-forming gas in the galactic disk if we make the standard assumption that the observed central velocity of the line is due to differential galactic rotation. The l - v diagrams plotted for the low-resolution and high-resolution survey data (Fig. 3a & b) show that the carbon line emission arises from gas located at galactocentric distances beyond 3.7 kpc. The line-forming gas at longitudes $\leq 50^\circ$ is confined between galactocentric distances of 3.7 kpc and 7.0 kpc. Moreover, line emission in the low-resolution survey for longitudes $\leq 50^\circ$ shows, in general, some confinement to the spiral arms. The galactic rotation model used here has been taken from Burton & Gordon (1978) after scaling it to $R_\odot = 8.5$ kpc and $\theta_0 = 220$ km s $^{-1}$. Fig. 4 shows the location of the line-forming regions obtained from the low-resolution survey in the plane of our Galaxy between $l = 4^\circ$ to 20° . These regions have been placed at the near kinematic distance. This is a reasonable assumption since the large beam width ($2^\circ \times 2^\circ$) of the low-resolution survey is likely to make the observations more sensitive to nearby regions. From the figure, it appears that most of the carbon line-forming gas in this longitude range is associated with spiral arm 3. Only toward $l = 9^\circ.3$, the near kinematic distance places the line emitting region near spiral arm 2. No line emission is detected from spiral arm 1 in this longitude range. In the high-resolution survey, line

emission is detected over a wider velocity range between $l = 0^\circ$ and 40° compared to that in the low-resolution survey (Fig. 3). In general, the velocity range over which carbon lines near 327 MHz are detected in the surveys is similar to the velocity spread of spiral arm tracers, for example, hydrogen RRLs near 3cm from H II regions (Lockman 1989). No line emission is detected from spiral arm 4 in the longitude range 20° to 89° in both surveys. A few line detections in this longitude range have velocity close to the tangent points. This is also a feature seen in the l - v diagram of spiral arm components in this longitude range (see, for example, 3cm RRL emission from H II regions; Lockman 1989). In summary, the l - v diagram of carbon line emission displays several similarities with those of spiral arm tracers.

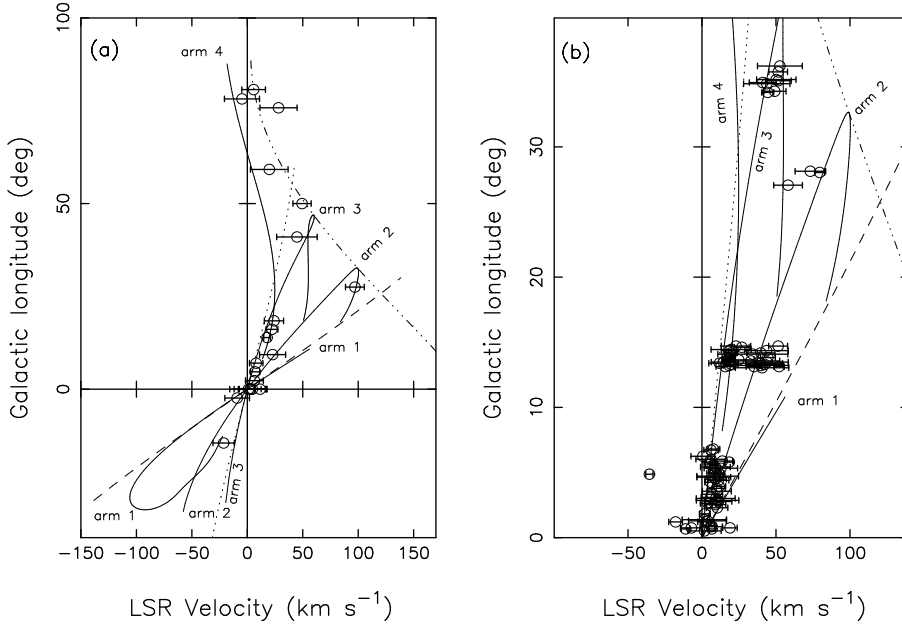


Fig. 3. Longitude-velocity ($l-v$) diagrams constructed from carbon RRL emission at 327 MHz data: (a) using data from low-resolution ($2^\circ \times 2^\circ$; paper I) survey; (b) using data from high-resolution ($2^\circ \times 6'$) survey. The marker indicates the central velocity whereas the length of the segment indicates the line width of the detected carbon lines. The four spiral arms (1 to 4 as designated by Taylor & Cordes (1993) are shown as solid lines in each of the $l-v$ diagrams. The dashed and dotted lines in each frame correspond to gas at galactocentric distances of 3.7 kpc and 7 kpc respectively. The dash-dot-dot-dash line indicates the locus of tangent points.

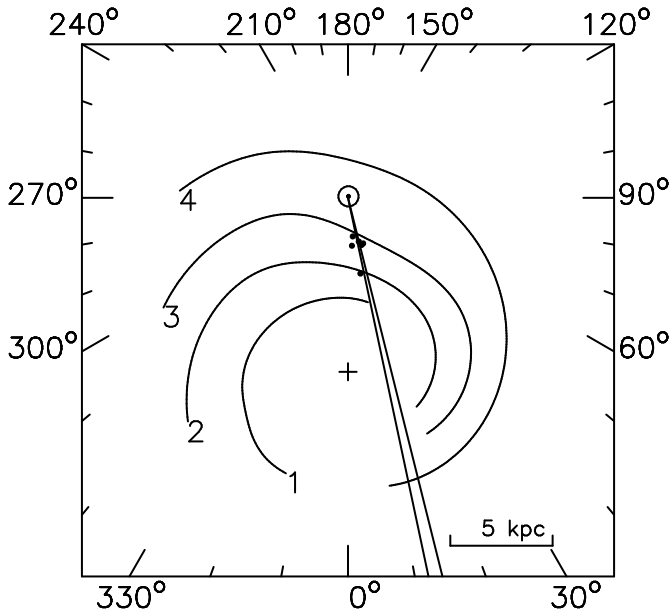


Fig. 4. Locations of the carbon line emitting regions (filled circles) between $l = 4^\circ$ to 20° are shown in galactocentric coordinates. The regions are placed at the near kinematic distances estimated using the observed central velocity of carbon line emission. Most of the detected carbon line forming regions in this longitude range lie in spiral arm 3. The region of the galactic disk covered by the 2° wide field centered at G13.9+0.0 is also shown. This region intercepts spiral arms 3, 2 and 4 at a distance ~ 1.9 , 3.7 and 14.1 kpc from the Sun.

We compared the l - v diagrams obtained from the 327 MHz survey with those obtained from the carbon absorption line data near 76 MHz (Erickson et al. 1995) and 35 MHz (Kantharia & Anantharamaiah 2001) since the observations at these three frequencies overlap in the longitude range $l = 332^\circ \rightarrow 20^\circ$. The l - v diagrams show similar features. At all the three frequencies, most of the detections are at longitudes $< 20^\circ$. The l - v diagrams obtained from the three observations indicate that the detected carbon line forming regions are confined between galactocentric distances of 3.7 to 8 kpc suggesting that they arise in the same diffuse C II regions. However, the width of lines detected in absorption in many cases are larger (up to a factor of 2) than that of emission lines observed in the low-resolution survey. The different line widths can be due to (a) different beam widths of the surveys and (b) effect of pressure and radiation broadening which have a strong dependence on the principal quantum number ($\propto n^{8.2}$ and $n^{8.8}$ respectively for widths in km s^{-1} ; Shaver 1975). Interestingly, the width of the absorption line seems to extend over the velocity range over which emission lines are observed in the high-resolution survey at the corresponding longitudes. Absorption lines near 76 MHz have been detected extensively at longitudes $340^\circ < l < 360^\circ$ for which we have few detections near 327 MHz. This is likely a case of lack of sensitivity (see

Section 3.1 for more details) than any intrinsic property of the line-forming regions. The general similarity of the l - v diagrams obtained from the three observations indicates that the carbon lines observed near 76 MHz and 35 MHz are the absorption counterparts of the carbon lines detected in emission near 327 MHz.

3.3. Radial Distribution

An l - v diagram gives a qualitative understanding of the distribution of ionized gas in the galactic disk. However, a more quantitative study can be made by computing the average emission as a function of the galactocentric radius. Since the ionized gas at “near” and “far” kinematic distance will be at the same galactocentric distance, the radial distribution is not affected by the two-fold ambiguity in estimating the line-of-sight distance. However the distribution will depend on several other factors: (a) the sensitivity of the observations to line-forming regions at different distances along the line-of-sight; (b) amplification of line intensity due to stimulated emission by galactic non-thermal background; (c) choice of the rotation model used for the computation.

The radial distribution of the different traces of the interstellar medium (Fig. 5) are computed using the method described in Paper I. In the computation for the carbon lines near 327 MHz, the Gaussian fits to the observed profiles were used instead of the actual spectra. This was necessary since the typical peak line intensity to RMS noise for a carbon line detection is only ~ 3 to 4. Using the Gaussian fit profile also eliminates any contamination from the hydrogen line emission, particularly for $R_{GC} < 2$ kpc. We have used the carbon line data from the low-resolution survey between $l = 4^\circ$ to 84° in the computation since in this longitude range other components of the ISM (H II regions and ^{12}CO emission) are well sampled and hence a direct comparison of their distribution with the carbon line data is possible.

The radial distribution obtained from the low-resolution survey carbon line data (see Fig. 5a) shows that the average emission extends from $R_{GC} = 2.5$ kpc to 9 kpc with a prominent peak near 6 kpc. About 90 % of the total observed carbon line emission originates between galactocentric distance 3.7 kpc and 8 kpc. The distribution falls off steeply on either side of the 6 kpc peak, the half width being 3.0 kpc. However, the true distribution is likely to be narrower than this because the broadening of the distribution due to intrinsic velocity dispersion has not been taken into account. An increase in line emission near 8.5 kpc is also seen which is due to the Cygnus loop region in the nearby Orion arm.

The spiral arm structure in the galactic disk should be evident in the radial distribution if the line emission shows some confinement to the spiral arms. In Fig. 5(b), the carbon line distribution computed using data in the longitude range, $l = 4^\circ$ to 20° is shown. Since most of the carbon line emission we detect is from this longitude range, it resem-

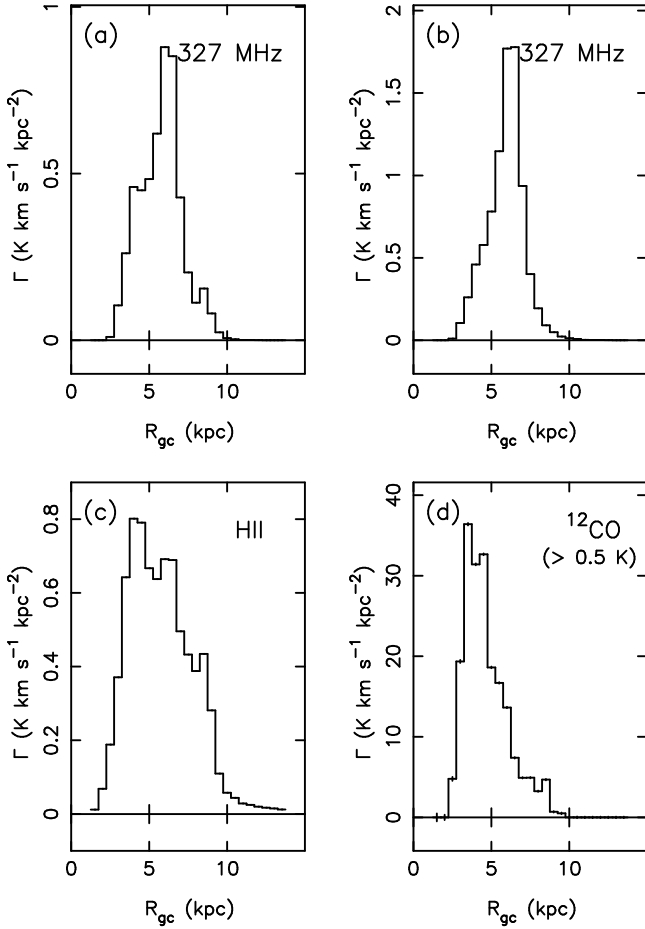


Fig. 5. The radial distribution (average emission Γ vs galactocentric radius R_{GC}) of different components of the ISM is shown in the figures. The radial distribution of (a) carbon RRL emission from the galactic plane near 327 MHz, (b) carbon RRL emission from the galactic plane near 327 MHz in the longitude range $l = 4^\circ$ to 20° , (c) hydrogen RRL emission from H II regions near 3 cm and (d) "intense" ($T_A > 0.5 \text{ K}$) ^{12}CO emission from the galactic plane. The radial distributions in (a), (c) & (d) were computed using the data in the longitude range $4^\circ < l < 84^\circ$ where all the components of the ISM are well sampled. The data are taken from Paper I (327 MHz carbon RRL), Lockman (1989) (RRLs from H II regions) and Dame et al. (1987) (^{12}CO).

bles the distribution in Fig. 5(a) with the prominent peak near 6 kpc clearly seen and the small peak near 8.5 kpc missing. As discussed in Section. 3.2, the line emission in this longitude range is likely to be confined to spiral arm 3, which naturally explains the peak at 6 kpc since the average distance to the spiral arm is $\sim 6 \text{ kpc}$. Comparing Figs. 5(a) and (b), it is seen that (a) shows slight excess emission near 4 kpc. Although there is no prominent peak in our low resolution data (Fig. 5(a)) there is some carbon RRL emission at 4 kpc distance associated with spiral arm 2. Moreover, we do detect emission from spiral arm 2 from several positions within this longitude range in our

high resolution survey data (see Fig 3b). Future higher resolution, sensitive observations are required to check the widespread presence of carbon line emission in spiral arm 2 in the inner Galaxy.

We compared the radial distribution of the carbon line emission with other components of the ISM to check for any similarities that may exist. We find that the radial distribution of carbon lines is distinct from that of H I. The latter is observed up to the outer reaches of the Galaxy (Burton 1988) whereas the carbon line emission is confined to galactocentric distances between 2.5 kpc to 9 kpc with well-defined peaks in its radial distribution. Comparing the radial distribution of carbon line emission with the distribution of the 3 cm hydrogen RRL emission from compact H II regions and "intense" ^{12}CO emission (Fig. 5c & d), both spiral arm tracers (Solomon, Sanders & Rivolo 1985), we find a number of similarities. Both, the 3 cm hydrogen RRL emission and ^{12}CO emission are confined (see Fig. 5c & d; for details see Paper I) in the range $R_{GC} = 2.5 \text{ kpc}$ to 9 kpc which is similar to the carbon line emission. A peak near 6 kpc is seen in the distribution of 3 cm hydrogen RRL emission and considerable ^{12}CO emission is present at the radial distance of 6 kpc, which is similar to that seen in the distribution of carbon line emission. We conclude that the carbon line emission near 327 MHz has similar galactic disk distribution as that of the star-forming regions. This result may appear somewhat different from what we know about the gas toward CasA – where the morphology of the carbon line forming gas resembles the distribution of H I observed in absorption across Cas A (Anantharamaiah et al. 1994) and no hydrogen RRL has been detected (Sorochenko & Smirnov 1993). However, it is not contradictory since in the inner Galaxy, the distribution of H I observed in absorption resembles that of ^{12}CO . H I with $\tau_{HI} > 0.1$ shows an 85 % probability of being associated with ^{12}CO emission (Garwood & Dickey 1989).

4. [C II] $158\mu\text{m}$ line emission from carbon RRL forming region

The [C II] $158\mu\text{m}$ line is due to the radiative decay of the fine structure transition $2P_{3/2} \rightarrow 2P_{1/2}$ in singly-ionized carbon. Recombination lines of carbon are a result of electronic transitions in a recombined atom in ionized gas. The excitation temperature of the fine structure transition ($\sim 91 \text{ K}$) is comparable to a subset of the temperatures which explain the observed low frequency carbon RRL emission (Kantharia & Anantharamaiah 2001). Moreover, dielectronic-like recombination (Watson, Western & Christensen 1980) is a process involving the excitation of the fine-structure levels which modifies the electronic level populations in recombined carbon; thus modifying the observed line optical depths of the carbon recombination lines. Since the two emission mechanisms are intricately linked, it is interesting to study their correlation.

In this section, we estimate the expected [C II] $158\mu\text{m}$ emission strength from low frequency carbon RRL-forming regions and compare the galactic distribution of the diffuse [C II] $158\mu\text{m}$ fine structure line with the carbon RRLs detected near 327 MHz.

4.1. The [C II] $158\mu\text{m}$ emission from the 327 MHz carbon RRL forming regions

The [C II] $158\mu\text{m}$ line originates predominantly from three types of regions: photodissociation regions (PDRs), cold neutral medium (CNM) and extended low-density warm ionized medium (ELDWIM) (Petuchowski & Bennett 1993, Heiles 1994). As described by Hollenbach et al. (1991), carbon is mostly in singly-ionized state upto $A_V < 4$ mag in low-density PDRs (the dense PDRs have a relatively low volume filling factor and hence may not contribute largely to the global diffuse [C II] $158\mu\text{m}$ emission). Hence low-density PDRs, which for the present discussion are considered as regions associated with molecular clouds, are possible sources of the diffuse fine structure line emission as well as carbon RRL emission. The CNM is another source of singly-ionized carbon. The CNM is distinct from PDRs in that they are predominantly atomic clouds with neutral densities $< 10^3 \text{ cm}^{-3}$ and typically $A_V \leq 1$ mag (Heiles 1994). The [C II] $158\mu\text{m}$ line is the major cooling transition in the CNM and the low-density PDRs since the number density of the colliding particles is generally less than the critical density, which depends on the colliding particles and their temperature. For temperatures relevant for CNM and low-density PDRs (~ 20 to 500 K), the critical densities due to collision with atoms and molecules are $\sim 3000 \text{ cm}^{-3}$ and $\sim 4000 \text{ cm}^{-3}$ respectively (Launay & Roueff 1977, Flower & Launay 1977). For densities larger than these, the fine-structure level is collisionally de-excited. In the ELDWIM, which consists of both the warm ionized medium (WIM; Reynolds 1993) and low-density ($n_e \sim 1 - 10 \text{ cm}^{-3}$) ionized gas in the inner Galaxy (Petuchowski & Bennett 1993, Heiles 1994), carbon is expected to be ionized. The critical density for collisions with electrons is $\sim 30 \text{ cm}^{-3}$ (Hayes & Nussbaumer 1984) assuming a temperature of 7000 K for the low-density ionized component (Anantharamaiah 1985). Roshi and Anantharamaiah (2001b) calculated a contribution of $8.1 \times 10^{-5} \text{ ergs s}^{-1} \text{ cm}^{-2} \text{ sr}^{-1}$ from the low-density ionized regions (one of the components of ELDWIM) in the longitude range $l = 0^\circ$ to 20° (relevant for the comparison between carbon RL and far-infrared line emission). The *diffuse* [C II] $158\mu\text{m}$ emission within $|b| < 2^\circ$ obtained from the higher resolution far-infrared line observations is $\sim 1.5 \times 10^{-4} \text{ ergs s}^{-1} \text{ cm}^{-2} \text{ sr}^{-1}$ (Nakagawa et al. 1998). Thus, the ELDWIM can contribute $\geq 54\%$ of the observed [C II] $158\mu\text{m}$ emission between $l = 0^\circ$ and 20° . However, ELDWIM is not a dominant source of 327 MHz carbon RRL emission since its temperature is high (line optical depth $\propto T_e^{-2.5}$) and carbon abundance is only depletion factor times the cosmic abundance (4×10^{-4} ; Spitzer

1978). Moreover, the ratio of the carbon to hydrogen line intensity detected in the 327 MHz survey is ~ 0.5 which is much higher than what is expected from the abundance ratio, suggesting a distinct origin for the two lines. The CNM and PDRs with their relatively low temperatures are envisaged as likely sites of origin for the 327 MHz carbon RRLs. Hence we estimate the contribution of the carbon RRL forming CNM and PDRs to the observed [C II] $158\mu\text{m}$ line intensity.

For estimating the intensity of the FIR line from carbon RRL forming regions, we considered typical parameters estimated for diffuse C II regions. Kantharia & Anantharamaiah (2001) have modeled the diffuse C II regions in a few directions in the inner Galaxy. They find that models with temperatures in the range $20 \rightarrow 80$ K can fit the observations depending on the angular extent of the line forming region. Even higher temperature (~ 150 K) models could fit the observations. Since the total H I column density (hence H I opacity) predicted by the higher temperature (~ 150 K) models are larger than that observed in the inner Galaxy, we use only models with temperatures in the range $20 \rightarrow 80$ K for the FIR line intensity calculation. The estimated electron density and path length corresponding to the observed integrated optical depth near 327 MHz of $\sim 0.01 \text{ km s}^{-1}$ in the inner Galaxy for this temperature range are $0.1 \rightarrow 0.03 \text{ cm}^{-3}$ and $0.2 \rightarrow 20 \text{ pc}$ respectively. The temperatures and electron densities which explain the low frequency carbon RRLs are encountered in the CNM (Heiles 2001) as well as low-density PDR (Hollenbach et al. 1991). If the line emission is associated with the CNM then the neutral density is $\sim 500 \rightarrow 150 \text{ cm}^{-3}$, which is the atomic density in these clouds. We assumed a carbon depletion factor of 0.5 for these estimates and other calculations presented here. The thermal pressure of these regions are $10000 \rightarrow 12000 \text{ cm}^{-3} \text{ K}$, which are not unreasonable for the CNM (Jenkins, Jura & Lowenstein 1983). The above numbers translate to hydrogen column densities ranging from $\sim 3.1 \times 10^{20} \rightarrow 9.3 \times 10^{21} \text{ cm}^{-2}$. Such column densities are not unreasonable in the inner Galaxy (Dickey & Lockman 1990). However toward the higher end, they cannot be reconciled with the observed width of the carbon lines (since they have to be shared by different CNM clouds). We discuss these issues in a later publication. Here, we consider the above possible physical conditions for diffuse C II regions coexisting with CNM.

As described above, the physical properties of carbon RRL forming region is also encountered in low-density PDRs. The regions with $A_V < 3$ mag of low-density PDR models of Hollenbach et al. (1991) have temperature similar to the higher temperature (~ 80 K) models of carbon RRL forming regions. Hydrogen is mostly atomic in these regions of the PDR. The neutral density of these regions should be $> 150 \text{ cm}^{-3}$ to produce the required electron density ($> 0.03 \text{ cm}^{-3}$) needed for the carbon RRL forming region. Typical observed H I column density of such regions associated with molecular clouds is $\sim 10^{20} \text{ cm}^{-2}$ (Wannier, Lichten & Morris 1983), which means several

such low-density PDRs are needed along a sight-line to produce the observed carbon RRL. The low-temperature (~ 20 K) “diffuse” C II regions could be zones with $A_V \sim 4$ mag of the PDR. For example, a low-density PDR model with $n_0 \sim 10^3 \text{ cm}^{-3}$ and incident FUV flux of $\sim 1.6 \text{ ergs cm}^{-2} \text{ s}^{-1}$ can have gas temperature ~ 20 K and electron density $\sim 0.1 \text{ cm}^{-3}$ at $A_V \sim 4$ mag (Hollenbach et al. 1991). Hydrogen is mostly molecular in these regions of the PDR. For the estimation of FIR line emission from $A_V \sim 4$ mag region, we use the above given parameters for the low-density PDR, which are typical values in the inner Galaxy. The H I density for this model is $\sim 10 \text{ cm}^{-3}$ and molecular density is $\sim 1000 \text{ cm}^{-3}$ (see Fig 4a of Hollenbach et al. 1991).

The intensity of the [C II] $158\mu\text{m}$ line from the neutral regions is given by (Bennett et al. 1994, Watson 1982)

$$I_{\text{C II}} = 7.416 \times 10^{-3} \frac{\frac{g_u}{g_l} e^{-h\nu/kT}}{1 + \frac{g_u}{g_l} e^{-h\nu/kT} + \left[\sum \frac{n_i}{n_{\text{cr}_i}} \right]^{-1}} n_{\text{C}^+} L, (2)$$

where $g_u (= 4)$, $g_l (= 2)$ are the statistical weights of $2P_{3/2}$ and $2P_{1/2}$ states respectively, $h\nu = 1.26 \times 10^{-14} \text{ ergs}$ is the energy of the $158 \mu\text{m}$ photon, k is the Boltzmann constant, T is the gas temperature in K, $n_{\text{C}^+} L$ is the column density of ionized carbon in $\text{cm}^{-3} \text{ pc}$. The above equation has been derived assuming an optically thin line from a two energy state atom. The population of energy states are determined by collisions and spontaneous emission in the optically thin case. In the above equation n_i is the density of colliding particles. n_{cr_i} is the critical density, which is defined as the ratio of the collision rate to the spontaneous emission rate. n_{cr_i} depends on the temperature of the interacting particles. For the temperatures encountered in the carbon RRL forming region $n_{\text{cr}_i} \sim 10 \text{ cm}^{-3}$ for electron collision (Hayes & Nussbaumer 1984) and 3000 and 4000 cm^{-3} for neutral hydrogen and molecular hydrogen respectively as described earlier.

We calculate the expected intensity of the [C II] $158\mu\text{m}$ emission from the CNM and PDR at temperatures of 20 K to be $5.2 \times 10^{-7} \text{ ergs s}^{-2} \text{ cm}^{-2} \text{ sr}^{-1}$ and $6.2 \times 10^{-7} \text{ ergs s}^{-2} \text{ cm}^{-2} \text{ sr}^{-1}$ respectively. For temperatures of 80 K, the expected intensity of the fine-structure line from CNM and PDR is found to be $1.4 \times 10^{-4} \text{ ergs s}^{-2} \text{ cm}^{-2} \text{ sr}^{-1}$. Comparing these estimates with what the Balloon-borne Infrared Carbon Explorer (BICE) observed in the inner Galaxy for $|b| < 1^\circ$ (Nakagawa et al. 1998), it appears that for temperatures near 20 K, the contribution to the total observed [C II] $158\mu\text{m}$ intensity is a negligible 0.4 % whereas if the temperatures of the C II regions are near 80 K, then 95 % of the total observed [C II] $158\mu\text{m}$ intensity can arise in the diffuse C II regions coexistent with CNM or low-density PDRs. Thus, if the temperature of the carbon RRL forming regions is low (~ 20 K), then most of the fine-structure line emission is likely to arise elsewhere – either in the ELDWIM or CNM and low-density PDR that do not produce observable carbon RRLs. If the temperature is high ($\sim 80\text{K}$), then most of the fine-structure

emission is likely to come from the PDRs and CNM that form the same family of diffuse C II regions which give rise to the low frequency carbon RRLs. In that case a more accurate estimate of the physical properties of the carbon RRL forming region is required to determine the relative importance of ELDWIM and PDRs/CNM to the global contribution of [C II] $158\mu\text{m}$ line emission. This will be attempted in future with multi-frequency carbon RRL data.

We note that in the inner Galaxy the assumption that the [C II] $158\mu\text{m}$ emission is optically thin is not entirely true. The opacity of the [C II] $158\mu\text{m}$ line is ~ 0.9 for a typical carbon RRL width of 14 km s^{-1} (Heiles 1994) arising in a cloud with temperature 80 K in the inner Galaxy. However, for simplicity and to get a first order estimate, we have considered the optically thin case which gives us the interesting results discussed above.

4.2. Longitudinal distribution of the carbon FIR line and radio line

We also attempted a comparison of the longitudinal distribution of the two tracers of ionized carbon. This is relevant since, as discussed in the previous subsection, a considerable fraction of the fine-structure line can be accounted for by the diffuse C II regions observed in low frequency carbon RRLs under certain physical conditions. If the longitudinal distributions of the two tracers are similar, it would support the higher temperature (~ 80 K) models for the carbon RRL forming regions and a substantial fraction of the observed [C II] $158\mu\text{m}$ emission is likely to arise in the carbon RRL forming region.

Wright et al. (1991) and Bennett et al. (1994) have presented the galactic distribution of the [C II] $158\mu\text{m}$ line with an angular resolution of $\sim 7^\circ$ using the data from the Far-Infrared Absolute Spectrophotometer (FIRAS) aboard the Cosmic Microwave Background Explorer (COBE). Bennett et al. (1994) report strong [C II] $158\mu\text{m}$ emission in the galactic plane with a half-intensity longitude range of $\sim 360^\circ \rightarrow 40^\circ$. A peak in the FIR emission is seen near $l = 80^\circ$ which matches with a peak seen in our 327 MHz RRL data. Bennett et al. (1994) caution against over-interpreting this peak due to few measurements in that region. Although the angular resolutions of the two datasets are different, a comparison of the gross distribution shows that the [C II] $158\mu\text{m}$ emission is more widespread than the carbon RRLs near 327 MHz (see Fig 2). Nakagawa et al. (1998) have used the data from BICE with a much finer angular resolution of $15'$. Their survey covers the region from $l = 350^\circ \rightarrow 25^\circ$. They detect [C II] $158\mu\text{m}$ emission in this longitude range from both “compact” and “diffuse” regions. The “diffuse” [C II] $158\mu\text{m}$ emission is observed to extend almost uniformly till the longitude limits of their observations in the galactic plane. In slight contrast, carbon RRLs near 327 MHz have been detected almost contiguously between $l = 0^\circ$ to 20° . We do not detect carbon RRLs

in the fourth quadrant (up to $l \sim -15^\circ$) due to reduced sensitivity of the equatorially-mounted Ooty Radio Telescope. Nakagawa et al. (1998) also observed reduced [C II] $158\mu\text{m}$ emission in regions adjacent to the galactic center up to about longitudes $\sim \pm 4^\circ$. This is a behavior distinct from our low-resolution survey carbon RRL data which shows comparable integrated optical depths in the galactic plane from $l = 0^\circ$ till $l = +10^\circ$ (see Fig 2).

In summary, intense FIR emission in the galactic plane is observed in the longitude range where carbon RRL near 327 MHz is detected. But the FIR emission seems to be more widespread in the galactic plane. Note that the comparison is, however, limited by (1) the large difference in the sensitivity of the FIR and carbon RRL observations; (2) poor velocity resolution of the existing FIR data. A comparison of the LSR velocities of the two tracers is essential in further establishing any connection between the two spectral lines. We therefore conclude that the “diffuse” C II regions can significantly contribute to the [C II] $158\mu\text{m}$ emission in the inner region of the Galaxy.

5. Latitude extent of Carbon line emission

We examined the data collected along galactic latitude toward two longitudes ($l = 0^\circ.0$, Fig 6 and $l = 13^\circ.9$, Fig 7) in the low-resolution survey. The beam center was shifted by half the beamwidth (i.e. 1°) along the galactic latitude and data was collected up to $b = \pm 4^\circ$ toward $l = 0^\circ$ and up to $b = \pm 3^\circ$ toward $l = 13^\circ.9$. The carbon feature is clearly seen in the spectrum averaged over the entire latitude range observed toward $l = 0^\circ$ (see Fig. 6c). The data toward the Galactic center was excluded since the carbon line emission in this direction is fairly strong and hence likely to dominate the averaged spectrum. Carbon lines are also detected when the data from positions separated by the beamwidth (i.e. 2°) over the entire sampled region are averaged, confirming the presence of carbon line emission over several degrees in galactic latitude.

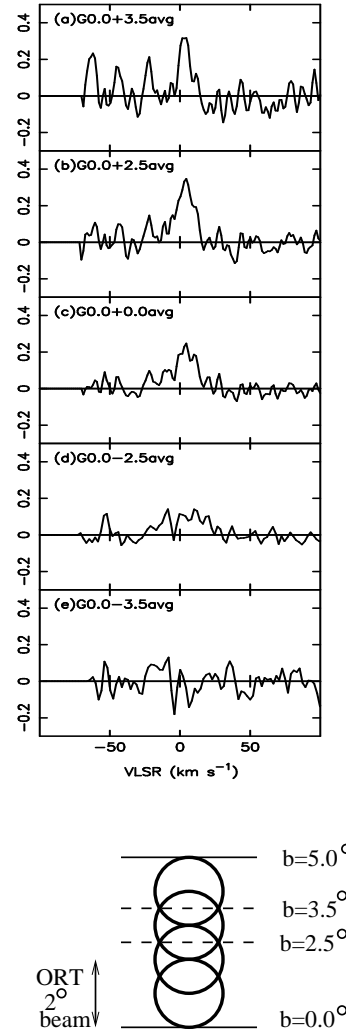


Fig. 6. Spectra of data averaged over different galactic latitude ranges toward $l = 0^\circ.0$ are shown in the top plot. The bottom schematic shows the stacking of the ORT beams along positive latitudes toward $l = 0^\circ.0$; similar data was also obtained for negative galactic latitudes. The spectra in the panels: a) G0.0+3.5avg was obtained by averaging data from beams centered at $b = 3^\circ, 4^\circ$ b) G0.0+2.5avg was obtained by averaging data over 5° from beams centered at $b = 1^\circ, 2^\circ, 3^\circ, 4^\circ$. c) G0.0+0.0avg was obtained by averaging data over 10° centered at $b = 0^\circ$. d) and e) are similar to b) and a) except that the data is averaged over negative latitudes. The spectrum toward the galactic center has been excluded from all the averaged spectra. The carbon line emission is seen to extend from $b \sim -2^\circ$ to $\sim 4^\circ$.

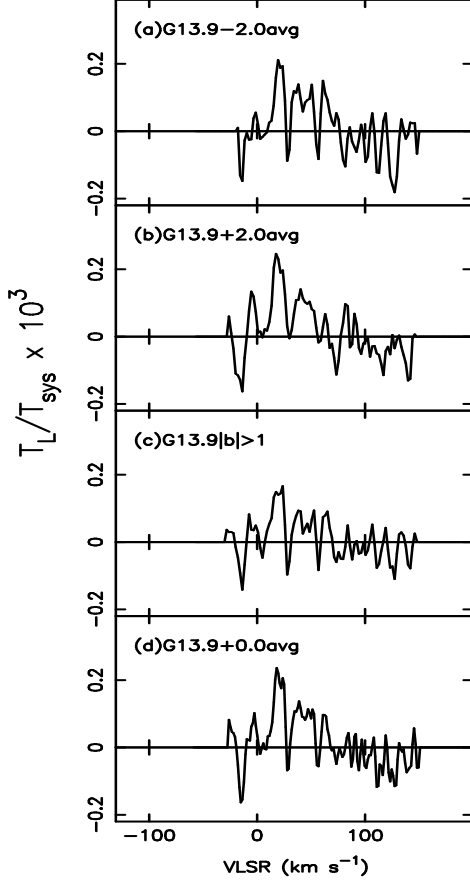


Fig. 7. Spectra obtained by averaging data over different galactic latitude range toward $l = 13^\circ.9$. Data is obtained up to $b = \pm 3^\circ$. a) G13.9-2.0avg is obtained by averaging the data over 4° in latitude about $b = -2^\circ$. b) G13.9+2.0avg is same as (a) but about $b = +2^\circ$. c) G13.9 $|b| > 1$ is the spectrum obtained by averaging all the data at latitude $|b| > 1^\circ$. The spectrum toward $l = 13^\circ.9$, $b = 0^\circ.0$ has been excluded in all the averaged spectra shown in the figure.

Table 2. Summary of the study of latitude extent of carbon line emission

<i>Position</i>	T_L/T_{sys}^1 $\times 10^3$	ΔV km s^{-1}	V_{LSR} km s^{-1}	V_{res}^4 km s^{-1}	RMS^2 $\times 10^3$	t_{int} hrs
Observations towards $l = 0^\circ.0$						
G0.0–2.5avg	0.13(0.02)	39.3(6.1)	4.3(2.6)	4.8	0.03	44.6
G0.0+2.5avg	0.32(0.03)	15.6(1.8)	2.9(0.7)	3.4	0.05	49.6
G0.0–3.0avg				7.6	0.03	32.1
G0.0+3.0avg	0.27(0.04)	12.5(2.2)	3.3(0.9)	3.4	0.06	37.7
G0.0–3.5avg				4.8	0.07	19.7
G0.0+3.5avg	0.34(0.06) ³	10.3(2.0)	2.8(0.8)	3.4	0.07	26.1
G0.0+0.0avg	0.20(0.02)	23.6(2.5)	2.7(1.0)	3.4	0.03	94.2
Observations towards $l = 13^\circ.9$						
G13.9–2.0avg	0.27(0.09) ³	9.2(3.5)	19.8(1.5)	4.8	0.09	29.0
G13.9+2.0avg	0.25(0.05)	11.0(2.5)	18.5(1.1)	4.8	0.05	30.8
G13.9 $ b > 1$	0.15(0.05) ³	10.0(3.8)	18.5(1.6)	4.8	0.05	38.6
G13.9+0.0avg	0.23(0.04)	9.5(2.0)	18.9(0.8)	3.4	0.05	59.8
	0.12(0.03)	26.6(6.9)	44.6(2.9)	3.4	0.05	59.8

¹ The line intensities are given in units of T_L/T_{sys} , where T_L is the line antenna temperature and T_{sys} is the system temperature

² RMS is in units of T_L/T_{sys} .

³ tentative detection.

⁴ The resolution to which the spectra are smoothed for estimating line parameters.

Our data indicates that the carbon line emission extends from $b \sim -2^\circ$ to $b \sim +4^\circ$ toward the galactic longitude $l=0^\circ$. The widths of the carbon lines seen in the positive latitude spectra and the negative latitude spectra (Fig. 6b & d) differ by a factor of ~ 2.5 . The line parameters are listed in Table 2. The difference in line width may indicate the presence of distinct line emitting regions along the latitude extent, maybe with different physical properties.

Fig. 7d shows the spectrum toward the longitude $l=13^\circ.9$ obtained by averaging the line emission along latitude between $b = \pm 3^\circ$. The spectrum toward $l=13^\circ.9$, $b = 0^\circ$ has been excluded in the average spectra shown in Fig. 7. A narrow feature ($\Delta V \sim 9 \text{ km s}^{-1}$) is clearly detected near 18.5 km s^{-1} . A weak, broad carbon line feature also seems to be present in the spectrum. The spectra averaged over the positive and negative latitude extents are shown in Figs. 7a & b. The narrow feature is clearly evident in these spectra; however the signal-to-noise ratio of this feature is low. This feature is also present in the spectrum shown in Fig. 7c, which is the average of all data at $|b| > 1^\circ$. The line parameters are listed in Table 2. The narrow carbon line emission is extended over, at least, the latitude range -3° to $+3^\circ$ suggesting the presence of a single large diffuse C II region. (see Section 6.2.1 for further discussion on the narrow carbon line emission.)

From the above two cases, we believe that the carbon line emitting gas in the inner Galaxy is spread over a galactic latitude extent of at least $b \sim \pm 3^\circ$.

6. Angular extent of carbon line-forming regions

Since only coarse resolutions are available at the low frequencies that diffuse C II regions can be studied using recombination lines and observations at different frequencies have different angular resolutions, it has been difficult to obtain definitive estimates of the angular and linear sizes of the diffuse C II regions. The ambiguity in the distances to these regions and the uncertainty in the angular size makes it difficult to obtain strict constraints on the linear size. Kantharia & Anantharamaiah (2001) modeled the carbon line data at three frequencies (35, 76 and 327 MHz) and obtained different physical models for different angular sizes of the line-forming region. They also attempted interferometric imaging of one position in the galactic plane in carbon recombination line using the VLA to obtain the angular extent of the line forming region. They obtained a lower limit on the angular size of $10'$. Clearly the angular size is an important parameter entering into the modeling of these regions and needs to be understood better. Since carbon lines are detected extensively in our low-resolution survey, it is likely that the diffuse C II regions are either 2° or more in angular extent or else consist of several small $\leq 2^\circ$ clumps within the beam. In this section we try to answer the question “do the line-forming regions consist of clumps with emission confined to small angular regions or is the emission ex-

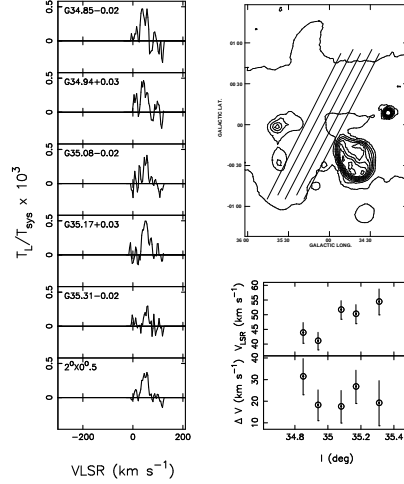


Fig. 8. Carbon line emission near $l = 35^\circ$. Top five panels on the left show the spectra observed with an angular resolution of $2^\circ \times 6'$ toward the positions marked on each frame and the lowermost panel shows the spectrum obtained by averaging the five spectra. The observed positions are marked by the slanted lines on the 11 cm continuum map from Reich et al. (1990). The slanted lines represent the $2^\circ \times 6'$ ORT beam. The LSR velocity and the width of the lines as a function of galactic longitude are shown in the plot on the right-hand side. The vertical bar represents the 3σ error in the estimated parameters.

tended and uniform over a large area ? ” We make use of the high-resolution data to answer this question.

6.1. Clumps in the diffuse C II regions

If the line emission arises in a homogeneous region with an angular extent of several degrees, then the line parameters observed at positions within this angular span are expected to be similar. Examination of the observed spectra in the high-resolution survey shows that at several positions there is considerable change in the line parameters when the beam center is shifted by $\sim 6'$ in declination. For example, the width of the observed carbon line toward the position G5.19+0.02 is $\sim 8 \text{ km s}^{-1}$ is about one-third the line width observed toward G5.33-0.03 ($\sim 23 \text{ km s}^{-1}$). The beam centers of the two positions are separated by $\sim 9'$. Another example is toward the direction $l = 35^\circ.1$ and $b = 0^\circ$ (see Fig. 8). Carbon line is clearly detected in the integrated spectrum obtained by averaging the high-resolution survey data over the longitude range $l = 34^\circ.85$ to $35^\circ.31$ ($0^\circ.5$ (along l) $\times 2^\circ$ (along b) region). However

on examining the five contiguous spectra (observed with a $2^\circ \times 6'$ beam) separated by $\sim 6'$, we find that the lines at positions with $l < 35^\circ$ have different central velocities compared to those at positions with $l > 35^\circ$ (see Fig. 8). Such behavior is exhibited toward many other positions separated by $\sim 6'$. This suggests that line emission in these directions arises from distinct diffuse C II regions or else that the diffuse C II regions have sub-structure on scales of $\sim 6'$. The near kinematic distance corresponding to the central velocity (48.6 km s^{-1}) of the integrated spectrum (Fig. 8) is 3.3 kpc, which is close to the line-of-sight distance to the spiral arm 3 at this longitude. If the angular extent of the clump at $l < 35^\circ$ is $\sim 6'$ then it corresponds to a linear size $\sim 6 \text{ pc}$ at the near kinematic distance. It, therefore, is likely that the diffuse C II regions toward G35.1+0.0 consist of such small line-forming clumps.

6.2. Extended diffuse C II regions

A subset of our data also shows a behavior different from what we discussed in the previous section. The high resolution data within the longitude range $l = 1^\circ.75$ to $6^\circ.75$ (within Field 2) seems to indicate the occurrence of a single C II region extended over a region of angular size $\sim 5^\circ$ in longitude. A similar extended ($\sim 2^\circ \times 6^\circ$) C II region is also observed toward $l = 13^\circ.9$, $b = 0^\circ$ (Field 3). These extended C II regions are discussed in detail below.

6.2.1. Carbon Line Emission toward Field 2

Here we examine the line emission seen from part of the 6° wide Field 2 ($l = 1^\circ.75$ to $6^\circ.75$) that we mapped using the high resolution data. Most of the high-resolution spectra from this region detected a $\sim 14 \text{ km s}^{-1}$ wide carbon line centered on $\sim 8 \text{ km s}^{-1}$. To improve the signal-to-noise ratio of the line emission from the extended C II region, we averaged the spectra over a region 1° (along l) \times 2° (along b). The averaged spectra are shown in Fig. 9. The $\sim 14 \text{ km s}^{-1}$ wide component is clearly seen in all the spectra. Table 6.2.1 gives the line parameters obtained from Gaussian fits to the spectra. The large angular extent of the $\sim 14 \text{ km s}^{-1}$ wide component is also evident from the detection of this component in the low-resolution observations toward G2.3+0.0, G4.7+0.0 and G7.0+0.0 (see Fig 9) with almost the same line parameters. The near kinematic distance corresponding to the central velocity of 8 km s^{-1} at $l = 5^\circ$ (for $l < 4^\circ$ the estimated distance increases) is $\sim 2.5 \text{ kpc}$. A 5° wide cloud at a distance of 2.5 kpc would have a physical size of $\sim 220 \text{ pc}$. This is a fairly large diffuse C II region.

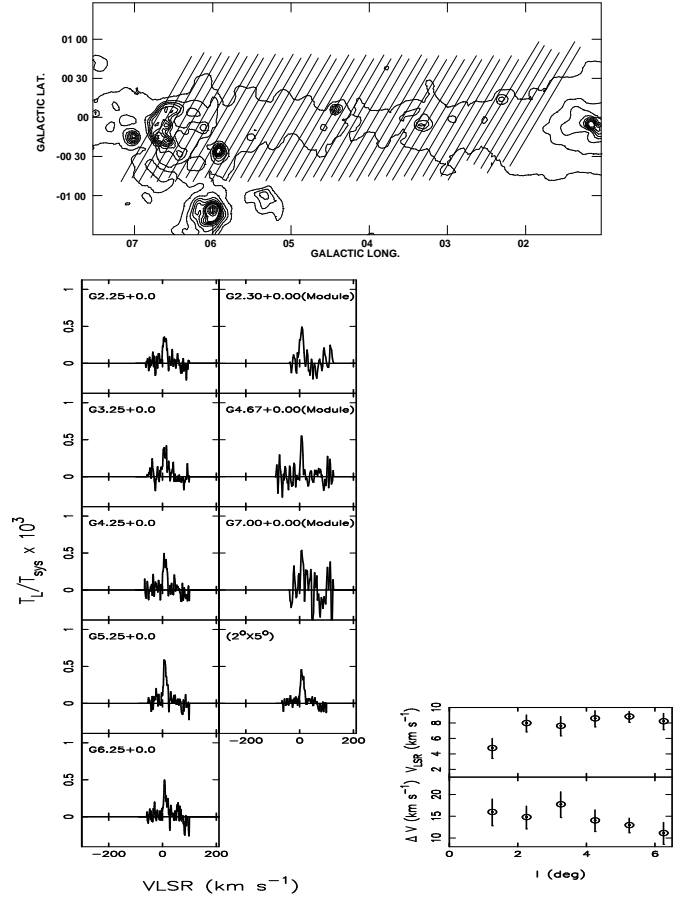


Fig. 9. Carbon line emission toward a 5° (along l) wide region centered at $l = 4^\circ.25$ and $b = 0^\circ$. The spectra shown in the panels in the first column are obtained by averaging the high-resolution ($2^\circ \times 6'$) survey data over a $2^\circ \times 1^\circ$ area centered on the galactic coordinates indicated in each frame. The top three spectra in the second column are from the low-resolution ($2^\circ \times 2^\circ$) survey, observed toward the galactic coordinates indicated in each frame. The lowermost spectrum in the second column is obtained by averaging the high-resolution survey data over the 5° wide region. The LSR velocity and the width of the lines from the spectra averaged over a $2^\circ \times 1^\circ$ region, as a function of galactic longitude are shown in the right-hand side plot. The vertical bars represent the 3σ error in the estimated parameters. The narrow feature near 8 km s^{-1} is observed in all the spectra indicating that the line-forming region is fairly extended in the sky plane. The observed positions are marked by the slanted lines on the 11 cm continuum map from Reich et al. (1990). The slanted lines represent the $2^\circ \times 6'$ beam of the ORT.

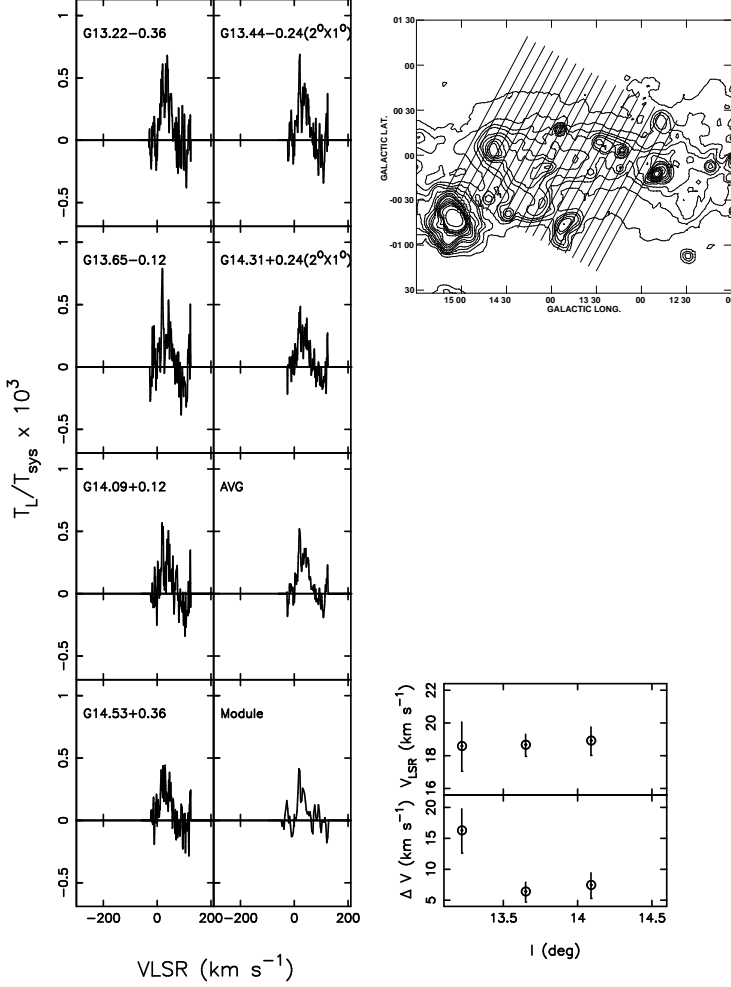


Fig. 10. Carbon line emission toward a 2° (along l) wide region centered at $l = 13^\circ.9$ and $b = 0^\circ$. The spectra on the left are obtained by averaging the high-resolution ($2^\circ \times 6'$) survey data over a $2^\circ \times 0^\circ.5$ region centered at the galactic coordinates indicated in each frame. The top two spectra on the right are obtained by averaging the data over $2^\circ \times 1^\circ$ region and that labeled “AVG” is obtained by averaging the data over the 2° region. The spectrum marked “Module” is from the low-resolution ($2^\circ \times 2^\circ$) survey toward $l = 13^\circ.9$ and $b = 0^\circ$. The LSR velocity and the line width using the spectra averaged over a $2^\circ \times 0^\circ.5$ region, as a function of galactic longitude are shown in the plot on the right-hand side. The vertical bars represent the 3σ error in the estimated parameters. The narrow component is observed in all the spectra with the same central velocity indicating the presence of an extended diffuse C II region. The observed positions are marked by the slanted lines on the 11 cm continuum map from Reich et al. (1990). The slanted lines represent the $2^\circ \times 6'$ beam of the ORT.

Table 3. Summary of the study of angular extent of carbon line emission in field 2

<i>Position</i>	T_L/T_{sys}^1 $\times 10^3$	ΔV (km s ⁻¹)	V_{LSR} (km s ⁻¹)	V_{res}^3 (km s ⁻¹)	RMS ² $\times 10^3$	t_{int} (hrs)
Average over 2° × 1°						
G2.25+0.0	0.35(0.04)	14.7(1.8)	7.9(0.7)	2.1	0.07	95.9
G3.25+0.0	0.36(0.03)	17.7(2.0)	7.6(0.8)	2.1	0.07	85.4
G4.25+0.0	0.37(0.04)	14.0(1.7)	8.5(0.7)	2.1	0.07	93.7
G5.25+0.0	0.51(0.04)	12.9(1.1)	8.8(0.5)	2.1	0.07	84.8
G6.25+0.0	0.36(0.05)	11.1(1.7)	8.2(0.7)	2.1	0.08	64.2
Average over 2° × 5°						
G4.25avg	0.39(0.02)	14.4(0.9)	8.6(0.4)	2.1	0.04	424

Table 4. Summary of the study of angular extent of carbon line emission in field 3

<i>Position</i>	T_L/T_{sys}^1 $\times 10^3$	ΔV (km s ⁻¹)	V_{LSR} (km s ⁻¹)	V_{res}^3 (km s ⁻¹)	RMS ² $\times 10^3$	t_{int} (hrs)
Average over 2° × 0°.5						
G13.22−0.36	0.41(0.09)	8.7(2.1)	50.9(0.9)	1.8	0.13	43.6
	0.57(0.08)	11.1(1.7)	36.5(0.7)	1.8	0.13	43.6
	0.50(0.06)	16.2(2.4)	18.6(1.0)	1.8	0.13	43.6
G13.65−0.12	0.33(0.05)	32.4(5.4)	42.4(2.3)	1.8	0.14	46.3
	0.73(0.11)	6.3(1.1)	18.6(0.5)	1.8	0.14	46.3
G14.09+0.12	0.48(0.08)	7.4(1.4)	18.9(0.6)	1.8	0.11	43.9
	0.30(0.04)	22.3(3.8)	40.9(1.6)	1.8	0.11	43.9
G14.53+0.36	0.33(0.04)	28.3(3.5)	23.3(1.5)	1.8	0.10	49.1
	0.24(0.05)	12.6(3.3)	48.5(1.4)	1.8	0.10	49.1
Average over 2° × 1°						
G13.44−0.24	0.36(0.03)	40.6(4.4)	36.8(1.9)	1.8	0.11	89.9
	0.48(0.09)	5.9(1.3)	18.5(0.5)	1.8	0.11	89.9
G14.31+0.24	0.25(0.06)	8.5(2.3)	17.8(1.0)	1.8	0.09	93.0
	0.27(0.03)	38.5(4.5)	35.8(1.9)	1.8	0.09	93.0
Average over 2° × 2°						
G13.88+0.00	0.32(0.02)	41.5(2.8)	36.7(1.2)	1.8	0.06	182.9
	0.35(0.04)	6.8(1.0)	18.4(0.4)	1.8	0.06	182.9

¹ The line intensities are given in units of T_L/T_{sys} , where T_L is the line antenna temperature and T_{sys} is the system temperature

² RMS is in units of T_L/T_{sys} .

³ The resolution to which the spectra are smoothed for estimating the line parameters.

¹ The line intensities are given in units of T_L/T_{sys} , where T_L is the line antenna temperature and T_{sys} is the system temperature

² RMS is in units of T_L/T_{sys} .

³ The resolution to which the spectra are smoothed for estimating the line parameters.

6.2.2. Carbon Line Emission toward Field 3

Within the 2° wide field centered at $l = 13^\circ.9$, $b = 0^\circ$, 20 positions were observed with a $2^\circ \times 6'$ beam as shown in Fig. 10. To improve the signal-to-noise ratio on the line emission from any extended C II region we averaged the data over a $2^\circ \times 0^\circ.5$ region. The resultant spectra are shown in the left hand side panels of Fig. 10. The carbon line in the spectra is clearly composed of a narrow and a broad component. These spectra were further integrated over two sets of 10 positions giving a spectrum of a region which is $2^\circ \times 1^\circ$ large. These two spectra are shown in the top two right hand side panels. The observed carbon line profile is well-fitted by a narrow ($\Delta V = 7 \text{ km s}^{-1}$) and a broad ($\Delta V = 42 \text{ km s}^{-1}$) Gaussian. Detailed line parameters obtained from the Gaussian fits are listed in Table. 4. In the lower two right hand side panels of Fig. 10, the high resolution spectra averaged over a 2° region and the low resolution spectrum over the same region are shown. The two spectra match well within errors and clearly show the presence of the two components. Since the wide component is likely to be a blend of many narrow components with slightly different velocities, we require more sensitive and higher angular resolution observations to resolve the broad component into the individual components. The narrow component is likely to arise in a single cloud which is at least 2° in extent along galactic longitude. Moreover, the gas toward this longitude has a latitude extent of $\pm 3^\circ$ (see Section 4) and the spectra toward $b \neq 0^\circ$ shows the presence of a narrow component (see Fig. 7) with almost similar line parameters as those obtained for the narrow component toward this direction in the Galactic plane. A slight increase in line width observed at higher latitudes might be a result of the poor signal-to-noise ratio of the spectra at higher latitudes compared to those near $l = 0^\circ.0$, which makes the Gaussian decomposition of the broad and narrow features somewhat uncertain. Thus, it appears that the diffuse C II region in this direction is extended over $\sim 6^\circ$ in latitude and at least 2° in longitude.

The line-of-sight toward this longitude intercepts the spiral arms 3, 2 and 4 which are nominally located at radial distances of ~ 1.9 , 3.7 and 14.1 kpc respectively from the Sun (see Fig. 4). The near and far kinematic distances corresponding to the observed central velocity (18.4 km s^{-1}) of the narrow component are 2.3 and 14.2 kpc. If the cloud is located at the near distance and the angular extent of the narrow line emitting region is at least $2^\circ \times 6'$ then it corresponds to a physical size perpendicular to the line-of-sight $> 80 \times 200$ pc. This, again, is a fairly large diffuse C II region.

In summary, our data toward Field 2 and 3 indicate the presence of extended C II regions - extending over ~ 200 pc or more. Line emission from many other positions suggests that structure in diffuse C II regions on scales of ~ 6 pc is common.

7. Summary

The paper discusses the carbon line emission detected in the low-resolution (Paper I) and the high-resolution surveys (Paper II) of recombination lines near 327 MHz made in the galactic plane using the ORT. The observed carbon line parameters in the high-resolution survey are presented. The carbon lines observed in the surveys arise in diffuse C II regions unlike the high frequency ($\nu > 1 \text{ GHz}$) recombination lines which arise in the photo-dissociation regions associated with H II regions. Most of our carbon line detections are in the longitude range $l = 358^\circ \rightarrow 20^\circ$ with a few detections between $l = 20^\circ$ to 89° . At longitudes $l = 0^\circ$ and $13^\circ.9$, observations with a $2^\circ \times 2^\circ$ beam along galactic latitude indicate that line emission extends at least up to $b \sim \pm 3^\circ$.

The l - v diagram and radial distribution constructed using the carbon line data near 327 MHz show similarity with those obtained from the hydrogen RRLs near 3 cm from H II regions. The radial extent of carbon line emission also resembles that of “intense” ^{12}CO emission. These similarities suggest that the distribution of the carbon line forming regions resembles the distribution of star-forming regions in our Galaxy. The l - v diagram of carbon line emission near 327 MHz is similar to those obtained from the carbon lines detected in absorption at frequencies near 76 MHz (Erickson et al. 1995) and 35 MHz (Kantharia & Anantharamaiah 2001), indicating that the latter are the absorption counterparts of the carbon lines observed in emission near 327 MHz.

We estimated the [C II] $158\mu\text{m}$ intensity expected from low frequency carbon RRL forming regions coexistent with the CNM and low-density PDRs. The estimate was made using a subset of physical parameters ($T_e = 20 \rightarrow 80 \text{ K}$) determined by Kantharia & Anantharamaiah (2001) for the diffuse C II regions. Significant fraction ($\sim 95 \%$) of the observed FIR line emission can arise in CNM/low-density PDR if the temperature of the diffuse C II region is close to $\sim 80 \text{ K}$ whereas only a small fraction (0.4%) of the observed FIR line emission can be produced in regions with temperature near 20 K . We then compared the longitudinal distribution of the two tracers of ionized carbon in the inner Galaxy to investigate their common origin. Available data do not rule out the possibility that diffuse C II regions contribute significantly to the FIR line emission in the inner Galaxy. However, data with comparable angular and spectral resolutions are required to further investigate this possibility.

Analysis of our high resolution data shows that the diffuse C II regions exhibit structure over angular scales ranging from $\sim 6'$ to $\sim 5^\circ$. Toward $l = 35^\circ$ and several other directions, the diffuse C II regions exhibit structure over $\sim 6'$, manifested as different central line velocities and line widths. At $l = 35^\circ$ we estimated a linear size of ~ 6 pc for a clump when placed at the near kinematic distance. Thus, it is likely that there exist C II regions of this size (or smaller) or there exist clumps of this size embedded in a larger diffuse C II region. Toward $l = 13^\circ.9$,

a narrow ($\sim 7 \text{ km s}^{-1}$) carbon line emitting region with an angular extent $\geq 2^\circ$ in galactic longitude and $\sim \pm 3^\circ$ in galactic latitude has been observed. A similar extended diffuse C II region was identified toward $l = 4^\circ.25$, $b = 0^\circ$. The angular extent of this region is at least 5° along l and 2° along b . Such large angular sizes translate to physical sizes perpendicular to the sight-lines of $> 200 \text{ pc}$. These are fairly large diffuse C II regions. Thus, our data shows that the diffuse C II regions observed in the inner Galaxy display structure on scales ranging from a few parsecs to a couple of hundred parsecs.

The association of some of the observed carbon line emission near 327 MHz in the surveys with HI self-absorption features will be discussed in Roshi, Kantharia & Anantharamaiah (2002).

Acknowledgements. DAR thanks F. J. Lockman and D. S. Balser for the many stimulating discussions and helpful suggestions during the course of this work. NGK thanks Rajaram Nityananda for useful suggestions. We are grateful to late K. R. Anantharamaiah for his guidance and support, to which we owe much of the work we have accomplished in our careers. We thank the referee F. Wyrowski for his comments and suggestions which have improved the paper.

References

- Anantharamaiah K. R., 1985, *J. Astrophys. Astron.*, 6, 203
 Anantharamaiah K. R., Erickson W. C., Payne H. E., Kantharia N. G., 1994, *ApJ*, 430, 682
 Bennett, C. L., et al. , 1994, *ApJ*, 434, 587
 Blake D. H., Crutcher R. M., Watson, W. D., 1980, *Nature*, 287,707
 Burton, W. B., & Gordon, M. A. 1978, *A&A*, 63, 7
 Burton, W. B., 1988, in Verschuur G. H., Kellermann K. I., eds, *Galactic and Extragalactic Radio Astronomy*. Springer-Verlag, Berlin, p. 295
 Dame T. M., et al. , 1987, *ApJ*, 322, 706
 Dickey, J. M., Lockman, F. J., 1990, *ARA&A*, 28, 215
 Erickson W. C., McConnell D., Anantharamaiah K. R., 1995, *ApJ*, 454, 125
 Flower, D. R., Launay, J. M., 1977, *J. Phys. B.*, 10, 3673
 Garay, G., Gomez, Y., Lizano, S., Brown, R. L., 1998, *ApJ*, 501, 699
 Garwood, R. W., Dickey, J. M., 1989, *ApJ*, 338, 841
 Golynkin A. A., Konvalenko A. A., 1990, in *Radio Recombination Lines: 25 years of investigation*, Kluwer Academic Publishers, Dordrecht, Gordon M. A., Sorochenko R. L., eds., p209
 Hayes, M. A., Nussbaumer, H., 1984, *A&A*, 134, 193
 Heiles, C., 1994, *ApJ*, 436, 720
 Heiles, C., 2001, *ApJ*, 551, L105
 Hollenbach, D., Takahashi, T., Tielens, A. G. G. M., 1991, *ApJ*, 377, 192
 Hollenbach, D., Tielens, A. G. G. M., 1997, *ARA&A*, 35, 179
 Jenkins, E. B., Jura, M., Lowenstein, M., 1983, *ApJ*, 270, 88
 Kantharia N. G., Anantharamaiah K. R., Payne H. E., 1998, *ApJ*, 506, 758
 Kantharia N. G., Anantharamaiah K. R., 2001, *J. Astrophys. Astron.*, 22, 51
 Konvalenko A. A., Sodin L. G., 1981, *Nature*, 294,135
 Konvalenko A. A., 1984, *Sov. Astron. Lett.*, 10, 384
 Launay, J. M., Roueff, E., 1977, *J. Phys. B.*, 10, 879
 Lockman, F. J., 1989, *ApJS*, 71, 469
 Nakagawa, T., et al. , 1998, *ApJS*, 115, 259
 Payne H. E., Anantharamaiah K. R., Erickson W. C., 1989, *ApJ*, 341, 890
 Payne H. E., Anantharamaiah K. R., Erickson W. C., 1994, *ApJ*, 430, 690
 Petuchowski, S. J., Bennett, C. L., 1993, *ApJ*, 405, 591
 Reich W., Fürst E., Reich P., Reif K., 1990, *A&AS*, 85, 633
 Reynolds, R. J., 1993, *Back to the Galaxy*, S. S. Hold and F. Verter, AIP Conf. Proc., Vol. 278, p. 156
 Roelfsema, P. R., Goss, W. M., 1992, *A&ARv*, 4,161
 Roshi A. D., 1999, Ph.D Thesis, University of Pune
 Roshi A. D., Anantharamaiah K. R., 2000, *ApJ*, 535, 231 (Paper I)
 Roshi A. D., Anantharamaiah K. R., 2001a, *J. Astrophys. Astron.*, 22, 81 (Paper II)
 Roshi A. D., Anantharamaiah K. R., 2001b, *ApJ*, 557, 226
 Roshi, A. D., Kantharia, N. G., Anantharamaiah, K. R., 2002, in preparation
 Shaver, P. A., 1975, *Pramana*, 5, 1
 Solomon P. M., Sanders D. B., Rivolo A. R., 1985, *ApJ*, 292, L19
 Sorochenko, R. L., Smirnov, G. T., 1993, *Sov Astron Lett*, 19, 2
 Sorochenko, R. L., 1996, *A&AT*, 1996, 11, 199
 Spitzer, L., 1978, *Physical processes in the Interstellar Medium*, Wiley, New York
 Swarup, G., et al. 1971, *Nature Phy. Sci.*, 230, 185
 Taylor J., H., Cordes J., M., 1993, *ApJ*, 411, 674
 Tielens, A. G. G. M., Hollenbach, D., 1985, *ApJ*, 291, 722
 Wannier, P. G., Lichten, S. M., Morris, M., 1983, *ApJ*, 268, 727
 Watson, W. D., Western, L. R., Christensen, R. B., 1980, *ApJ*, 240, 956
 Watson, D. M., 1984, *Galactic and Extragalactic Infrared spectroscopy*, M. F. Kessler, J. P. Phillips (Dordrecht: Reidel), p. 195
 Wright, E. L., et al. 1991, *ApJ*, 381, 200
 Wyrowski, F., Walmsley, C. M., Goss, W. M., Tielens, A. G. G. M., 2000, *ApJ*, 543,245